Published in final edited form as:
Phys Med Biol. 2012 December 21; 57(24): 8185–8200. doi:10.1088/0031-9155/57/24/8185.

MR Chemical Exchange Imaging with Spin-Lock Technique (CESL): A Theoretical Analysis of Z-spectrum using a Two-Pool $R_{1\rho}$ Relaxation Model beyond the Fast-Exchange Limit

Jing Yuan[1], **Jinyuan Zhou**[2,3], **Anil T Ahuja**[1], and **Yi-Xiang J Wang**[1]

[1]Department of Imaging and Interventional Radiology, The Chinese University of Hong Kong, Shatin, New Territories, Hong Kong, China

[2]Department of Radiology, Johns Hopkins University School of Medicine, Baltimore, Maryland, USA

[3]F.M. Kirby Research Center for Functional Brain Imaging, Kennedy Krieger Institute, Baltimore, Maryland, USA

Abstract

Chemical exchange (CE) process has been exploited as a novel and powerful contrast mechanism for MRI, which is primarily performed in the form of chemical exchange saturation transfer (CEST) imaging. Spin-lock (SL) technique can also be used for CE studies, although traditionally performed and interpreted quite differently from CEST. Chemical exchange imaging with spin-lock technique (CESL), theoretically based on the Bloch-McConnell equations common to CEST, has potentials to be used as an alternative to CEST and to better characterize CE processes from slow and intermediate to fast proton exchange rates through the tuning of spin-lock pulse parameters. In this study, Z-spectrum and asymmetric magnetization transfer ratio (MTR_{asym}) obtained by CESL are theoretically analyzed and numerically simulated using a general two-pool $R_{1\rho}$ relaxation model beyond the fast-exchange limit. The influences of spin-lock parameters, static magnetic field strength B_0 and physiological properties on Z-spectrum and MTR_{asym} are quantitatively revealed. Optimization of spin-lock frequency and spin-lock duration for the maximum CESL contrast enhancement is also investigated. Numerical simulation results in this study are compatible with the findings in the existing literatures of CE imaging studies.

Keywords

Chemical exchange imaging with spin-lock technique (CESL); chemical exchange saturation transfer (CEST); spin-lock; $R_{1\rho}$; magnetization transfer

INTRODUCTION

MRI provides a variety of image contrasts to distinguish the diseased tissues from healthy tissues based on different mechanisms like relaxation times of T_1, T_2 and T_2^*, diffusion, and perfusion. Recently, chemical exchange (CE) has been exploited as a novel and powerful contrast enhancement mechanism in addition to normal MRI contrast mechanisms. The principle of CE based MRI relies on the proton exchange process between free water and biological molecules containing exchangeable labile protons resonating at a frequency

Corresponding Author: Jing Yuan, Ph.D., Department of Imaging and Interventional Radiology, The Chinese University of Hong Kong, Shatin, New Territories, Hong Kong, China, Tel: 852-2632-1036, jyuan@cuhk.edu.hk.

different from that of water. Proton exchange between them leads to the magnetization attenuation of water that is detectable by the means of normal MR acquisition method. Currently, CE based MRI is mostly performed in the form of chemical exchange saturation transfer (CEST) imaging (Ward *et al.*, 2000; van Zijl and Yadav, 2011). In CEST imaging, different irradiation frequencies of the long and weak saturation radiofrequency (RF) pulse are applied to obtain the signal intensity ratios compared to the unsaturated signal intensity as a function of frequency offset ($\Delta\Omega$) with respect to water, often referred as the Z-spectrum. Quantitatively, the magnetization transfer ratio (MTR) is defined as:

$$MTR(\Delta\Omega)=1-M(\Delta\Omega)/M_0, \quad (1)$$

where $M(\Delta\Omega)$ and M_0 denote magnetization or image intensity at frequency offset of $\Delta\Omega$ and without RF irradiation, respectively. To eliminate direct water saturation (DS) effect, asymmetric MTR is proposed as:

$$\mathrm{MTR}_{\mathrm{asym}}(\Delta\Omega)=\mathrm{MTR}(\Delta\Omega)-\mathrm{MTR}(-\Delta\Omega). \quad (2)$$

The voxel-wise map of asymmetric MTR is normally used to visualize the CE-based contrast for lesion detection and tissue characterization.

Spin-lock technique, traditionally applied for the study of relaxation time ($T_{1\rho}$) or relaxation rate ($R_{1\rho}$) in the rotating frame, could also be used for chemical exchange imaging. In traditional SL imaging, a stronger but much shorter spin-lock pulse than CEST imaging is applied, and the image intensities at different spin-lock pulse times (TSL) are fitted to a mono-exponential decay model to quantify $T_{1\rho}$ or $R_{1\rho}$:

$$M(TSL)=M_0\cdot e^{-TSL/T_{1\rho}}=M_0\cdot e^{-TSL\cdot R_{1\rho}}, \quad (3)$$

where $M(TSL)$ and M_0 denote the magnetization or image intensity at spin-lock times of TSL and zero, respectively. $T_{1\rho}$-weigthed image or $T_{1\rho}$ map has been widely used for many clinical applications involving various organs (Li *et al.*, 2008; Johannessen *et al.*, 2006; Borthakur *et al.*, 2008; Wang *et al.*, 2011). Actually, CE information could be reflected by $T_{1\rho}$ or $R_{1\rho}$ dispersion, which is the $T_{1\rho}$ or $R_{1\rho}$ change as a function of the spin-lock field strength B_{1SL} or spin-lock frequency FSL, where $FSL=\gamma B_{1SL}$ and γ is the gyromagnetic ratio of protons (42.576 MHz/T).

Despite the different acquisition and interpretation form by CEST and SL imaging, both offer chemical exchange information of physiological systems. CEST is normally described sensitive to the processes when the proton exchange rate is much smaller or comparable to the offset frequency of labile protons, often referred to slow or intermediate exchange, while SL imaging is considered to be more sensitive to probe fast proton exchange processes in which case the proton exchange rate is much larger than the offset frequency.

Unlike the SL imaging, CEST typically uses much lower RF pulse field strength and longer duration for the study of slow to intermediate CE processes (Jin *et al.*, 2012). In theory, the Bloch-McConnell equations form the theoretical basis for the quantitative analysis of chemical exchange for both. The underlying equivalence of spin-lock and CEST irradiation schemes has also been revealed (Zaiss and Bachert, 2012). Based on these equations, current CEST models can well describe slow CE processes in a simple form (van Zijl and Yadav, 2011; Zhou *et al.*, 2003b; Zhou *et al.*, 2003a). However, it becomes difficult to quantify intermediate or fast CE processes (Jin *et al.*, 2012) due to the extremely complicated form after extension (Zhou *et al.*, 2004). As comparison, the dynamic magnetization evolution under wide ranges of chemical exchange rates could be more conveniently quantified and interpreted by a general two-pool $R_{1\rho}$ relaxation model (Trott and Palmer, 2002).

In practice, the full acquisition of $T_{1\rho}$ dispersion by measuring $T_{1\rho}$ values at multiple FSLs to quantify proton exchange could be very time consuming even with the limited TSLs at each FSL for acceleration (Yuan *et al.*, 2012b), so usually not practical for routine patient scan. Meanwhile, unlike MTR_{asym} map for CEST, neither $T_{1\rho}$ map nor $T_{1\rho}$ dispersion curves straightforwardly visualize CE-based contrast on image. Therefore, analysis of Z-spectrum and MTR_{asym} obtained by spin-lock technique provides an efficient and intuitive mean for CE quantification and CE-based image contrast visualization, and has raised more research interests recently (Jin *et al.*, 2012; Jin *et al.*, 2011; Kogan *et al.*, 2012).

The purpose of this study is to theoretically investigate the Z-spectrum and asymmetric MTR of chemical exchange imaging with spin-lock technique (CESL) using the two-pool $R_{1\rho}$ model beyond fast-exchange limit (Trott and Palmer, 2002). The influences of various parmaeters, including SL parameters of FSL, TSL, static magnetic field strength B_0, offset of labile proton pool, proton exchange rate, population ratio of labile proton pools, as well as intrinsic relaxation time T_2, on Z-spectrum and asymmetric MTR are numerically simulated and quantitatively analyzed. Optimization to maximize the CE-based contrast by adjusting the spin-lock pulse parameters is investigated. The theoretical correlations between CEST models and $R_{1\rho}$ model are revealed.

METHODS

Theoretical Analysis

We consider a two-pool model that proton exchanges between pool A and Pool B with distinct Larmor frequencies of Ω_a and Ω_b, respectively. The population ratios of A and B are p_a and $p_b=1-p_a$, respectively. The resonance offsets in the rotating frame for A and B are expressed as:

$$\delta_a=\Omega_a-\omega_{rf} \quad \text{and } \delta_b=\Omega_b-\omega_{rf}, \quad (4)$$

where ω_{rf} is the transmitter frequency of the applied RF pulse. The first-order forward proton exchange rate from A to B and reverse proton exchange rate from B to A are defined as k_a and k_b. The total exchange rate is $k=k_a+k_b$. To achieve dynamic equilibrium, it is required that:

$$p_a \cdot k_a=p_b \cdot k_b. \quad (5)$$

By substituting $k=k_a+k_b$ and $p_a+p_b=1$ into Eq. [5]:

$$p_a=\frac{k_b}{k} \quad \text{and } p_b=\frac{k_a}{k}. \quad (6)$$

The proton exchange process is referred to slow, intermediate and fast if $k<<|\Omega_a-\Omega_b|$, $k\sim|\Omega_a-\Omega_b|$, and $k>>|\Omega_a-\Omega_b|$.

The Bloch-McConnell equations quantitatively describe the time evolution of the magnetization of pool A (M_a) and B (M_b) under proton exchange. When the RF pulse is applied in x direction, it is written as:

$$\frac{d}{dt}\begin{bmatrix} M_{ax} \\ M_{bx} \\ M_{ay} \\ M_{by} \\ M_{az} \\ M_{bz} \end{bmatrix} = \begin{bmatrix} -k_a - R_2 & k_b & -\delta_a & 0 & 0 & 0 \\ k_a & -k_b - R_2 & 0 & -\delta_b & 0 & 0 \\ \delta_a & 0 & -k_a - R_2 & k_b & -\omega_1 & 0 \\ 0 & \delta_b & k_a & -k_b - R_2 & 0 & -\omega_1 \\ 0 & 0 & \omega_1 & 0 & -k_a - R_1 & k_b \\ 0 & 0 & 0 & \omega_1 & k_a & -k_b - R_1 \end{bmatrix} \begin{bmatrix} M_{ax} \\ M_{bx} \\ M_{ay} \\ M_{by} \\ M_{az} \\ M_{bz} \end{bmatrix} + R_1 \begin{bmatrix} 0 \\ 0 \\ 0 \\ 0 \\ M_{a0} \\ M_{b0} \end{bmatrix} \quad (7)$$

where M_{a0} and M_{b0} are the original thermal equilibrium magnetization of A and B along the B_0 direction and t is the time. ω_1 is the Rabi frequency of the SL pulse and $\omega_1 = 2\pi\gamma B_{1SL} = 2\pi FSL$. γ is the gyromagnetic ratio of protons (42.576 MHz/T) and FSL is the spin-lock frequency. R_1 and R_2 are understood as population averaged spin-lattice and spin-spin relaxation rates. For the first-order linear differential equations shown in Eq. [7], $R_{1\rho}$ is derived as:

$$R_{1\rho} = -\lambda, \quad (8)$$

where λ is the largest real eigenvalue of the matrix in Eq. [7]. The detail derivation could be referred to the literature (Trott and Palmer, 2002). Assuming $R_2 - R_1 << k$, the general $R_{1\rho}$ model is expressed in a linearized from as given by:

$$R_{1\rho} = R_1\cos^2\theta + R_2\sin^2\theta + \frac{p_a p_b \delta^2 k \sin^2\theta}{\frac{\omega_{aeff}^2 \omega_{beff}^2}{\omega_{eff}^2} + k^2} = R_1\cos^2\theta + (R_2 + R_{ex})\sin^2\theta. \quad (9)$$

Eq. [9] is compatible with the result derived in the reference (Zaiss *et al.*, 2012). ω_{aeff}, ω_{beff} and ω_{eff} are the effective spin-lock frequencies in the rotating frame for pool A, B and bulk average, respectively. δ is the Larmor frequency difference between Pool A and B. Exchange relaxation rate R_{ex} reflects the relaxation variation due to chemical exchange. Relationships between parameters in Eq. [9] are listed as:

$$\omega_{aeff}^2 = \delta_a^2 + \omega_1^2 = \delta_a^2 + (2\pi \cdot FSL)^2 \text{ and } \omega_{beff}^2 = \delta_b^2 + \omega_1^2 = \delta_b^2 + (2\pi \cdot FSL)^2, \quad (10)$$

$$\delta = \delta_b - \delta_a = \Omega_b - \Omega_a, \quad (11)$$

$$\Delta\Omega = p_a\Omega_a + p_b\Omega_b - \omega_{rf}, \quad (12)$$

$$\omega_{eff}^2 = \Delta\Omega^2 + \omega_1^2 = \Delta\Omega^2 + (2\pi \cdot FSL)^2, \quad (13)$$

$$\theta = \arctan\left(\frac{\omega_1}{\Delta\Omega}\right) = \arctan\left(\frac{2\pi \cdot FSL}{\Delta\Omega}\right), \quad (14)$$

where $\Delta\Omega$ is the offset frequency of the spin-lock pulse with respect to the population averaged Larmor frequency. Note that Eq. [9] is generally valid for description of slow, intermediate and fast proton changes and has no assumption on the ratio of pool population. It is only required for the derivation that $R_2 - R_1 << k$. Considering that most biological tissues have T_2 longer than 40ms (Stanisz *et al.*, 2005), quite independent of B_0, and much longer T_1 than T_2, quantification by Eq. [9] is still accurate even for very slow exchange rates.

Under the application of a spin-lock pulse, magnetization along the effective spin-lock field direction would decay at the rate of $R_{1\rho}$ to a steady state. The magnetization evolution is written as:

$$M=(M_0 - M_{ss}) \cdot e^{-R_{1\rho} \cdot TSL} + M_{ss}, \quad (15)$$

where M_{ss} is the steady-state magnetization. By using the normal Bloch equations with $dM_{ss}/dt=0$, it can be derived that (Jin *et al.*, 2012; Desvaux and Berthault, 1999):

$$M_{ss}=M_0 \cdot \frac{R_1 \cdot \cos\theta}{R_{1\rho}} \quad \text{if } R_2^2 \ll \omega_1^2+\Delta\Omega^2. \quad (16)$$

Note that relevant parameters like R_1, θ, and M_0 in Eqs. [15–16] are understood as population averaged values.

By substituting Eq. [9] and Eq. [16] into Eq. [15], Z-spectrum obtained by a spin-lock pulse could be analytically expressed as:

$$\begin{aligned}\frac{M}{M_0} &= 1 - MTR(TSL, FSL, \Delta\Omega) \\ &= \left(1 - \frac{R_1 \cdot \cos\theta}{R_{1\rho}}\right) \cdot e^{-R_{1\rho} \cdot TSL} + \frac{R_1 \cdot \cos\theta}{R_{1\rho}} \\ &= \left(1 - \frac{R_1 \cdot \cos\theta}{R_1\cos^2\theta+(R_2+R_{ex})\sin^2\theta} \cdot e^{-(R_1\cos^2\theta+(R_2+R_{ex})\sin^2\theta) \cdot TSL} + \frac{R_1 \cdot \cos\theta}{R_1\cos^2\theta+(R_2+R_{ex})\sin^2\theta}\right).\end{aligned} \quad (17)$$

Note MTR is expressed as a function of adjustable spin-lock parameters of TSL, FSL and ΔΩ, although in fact it is also dependent on many other factors. Accordingly, asymmetric MTR (MTR_{asym}) is given as:

$$MTR_{asym}(TSL, FSL, \Delta\Omega)=MTR(TSL, FSL, \Delta\Omega) - MTR(TSL, FSL, -\Delta\Omega). \quad (18)$$

Numerical Simulation

Numerical programs using MATLAB v7.9 (MathWorks, Natick, MA, USA) were developed to simulate the Z-spectrum obtained by the spin-lock technique. Z-spectrum and asymmetric MTR under the influence of B_0, spin-lock parameters including TSL, FSL and ΔΩ, and tissue properties including intrinsic relaxation times, pool population ratio, Larmor frequency difference between two pools and proton exchange rate, were individually investigated and illustrated. To acquire Z-spectrum that could be modeled by Eq. [17], the flip-down and flip-up angle α for spin-lock pulse should be adjusted at each offset frequency ΔΩ of the spin-lock pulse as $\alpha=\arctan(2\pi FSL/\Delta\Omega)$ to make sure that the magnetization is flipped to the nominal effective spin-lock field direction and experiences pure $T_{1\rho}$ relaxation along this direction. The deviation between the flipped magnetization and the effective spin-lock field strength induced by B_0 or B_1 inhomogeneities was not taken into account for simulation. In the simulation of Z-spectrum acquisition, a step of 0.01ppm (parts per million) of B_0 Larmor frequency (γB_0) was used to obtain the smooth MTR and

MTR_{asym} curves. In the illustration of Z-spectrum and MTR_{asym}, 0ppm corresponded to the B_0 Larmor frequency. Without losing generality, pool A could be considered as the pool of free water in biological tissues, on resonance with B_0 Larmor frequency. Pool B is the chemical exchange agent of interest containing labile protons, resonant at an offset frequency (δ_b) of 3ppm relative to pool A, such as Glutamate (Cai *et al.*, 2012). Pool population is assumed to be highly asymmetric with $p_a=0.99$ and $p_b=0.01$ for simulation unless particularly specified, similar to the normal tissue microenvironment with a large pool of water and a small pool of labile protons. Theoretical Z-spectra obtained at B_0 of 9.4T (~400MHz) were simulated unless particularly specified. The default proton exchange rate was assumed to be 500/s (or ~3143rad/s) in simulation unless particularly specified. The default spin-lock frequency and spin-lock time were set as 500Hz (corresponded to spin-lock field strength of ~11.74μT and angular frequency of ~3143rad/s) and 50ms, respectively.

Numerical simulation indicated that Z-spectrum and MTR_{asym} were relatively insensitive to the typical T_1 ranges (from a few hundred milliseconds to three thousand milliseconds) for various tissues at different B_0 for intermediate and fast exchange. Therefore, the effect of T1 on Z-spectrum was not shown in the results. The population averaged T_1 was assumed to be 1500ms for all simulations. However, the effect of population averaged T_2 on Z-spectrum and MTR_{asym} may not be negligible in the typical ranges for tissues (less than 100ms and relatively independent of B_0). The population averaged T_2 was assumed to be 80ms in simulations unless particularly specified.

RESULTS

Influence of spin-lock parameters on Z-spectrum and MTR_{asym}

Figure 1 shows the simulated Z-spectrum (a) and MTR_{asym} (b) under the applications of spin-lock pulses with different FSLs but a fixed TSL of 50ms at 9.4T. As shown in Fig. 1a, the saturation peak width of the Z-spectrum increases with FSL. When FSL is smaller than 100Hz ($FSL<<k$), MTR_{asym} is generally smaller than $0.02M_0$ that is obtained without spin-lock pulse, or when the spin-lock offset frequency Ω is set sufficiently far from the resonance. When FSL is comparable with k ($400<=FSL<=600$), MTR_{asym} is enhanced dramatically and the maximum MTR_{asym} is larger than $0.08M_0$. When FSL is even larger than 600Hz, the maximum MTR_{asym} begins to reduce with the increasing FSL. The variation of MTR_{asym} at 3ppm with FSL is illustrated in Fig. 1c. The maximum MTR_{asym} at 3ppm occurs at the FSL of 527Hz, close to the proton exchange rate k.

Figure 2 shows the influence of TSL on the Z-spectrum (a) and MTR_{asym} (b) at a fixed FSL of 500Hz. As seen in Fig. 2a, the longer the TSL, the more completely pool A is suppressed. With the TSL longer than 500ms, pool A is almost completely saturated by the on-resonance spin-lock pulse. However, the maximum MTR_{asym} does not monotonically increase with TSL (Fig. 2b). In addition, the location of the maximum MTR_{asym} is shifting to higher off-resonance with the increasing TSL, not always at 3ppm. The maximum MTR_{asym} could be over $0.2M_0$ when the TSL is optimized. Fig. 2c illustrates the variation of MTR_{asym} at 3ppm with TSL. The MTR_{asym} at 3ppm is maximized at the TSL around 350ms.

Influence of B_0 field strength on Z-spectrum and MTR_{asym}

The dependence of Z-spectrum and asymmetric MTR on the main magnetic field strength B_0 under the application of a spin-lock pulse with the FSL of 500Hz and the TSL of 50ms is shown in Fig. 3. The on-resonance saturation rate of pool A increases with B_0. The increase of absolute offset frequency in Hz of pool B with B_0 makes it easier to recognize pool B on the Z-spectrum, as indicated by the arrow. It is expected that a more pronounced saturation

of pool B closer to its offset frequency (3ppm) would appear on the overall Z-spectrum at an even stronger B_0, and hence leads to the enhanced MTR_{asym} and image contrast. As demonstrated in Fig. 3b, the maximum MTR_{asym} increases with B_0, with its location closer to 3ppm. Meanwhile, the shape width of the MTR_{asym} curve becomes narrower with B_0, indicating a higher specificity for the detection of pool B. Fig. 3c shows the monotonically increasing MTR_{asym} at 3ppm is always with the B_0 Larmor frequency, but with a slower increasing rate at higher B_0.

Influence of tissue properties on Z-spectrum and MTR_{asym}

Figure 4a shows the Z-spectra if pool B resonates at different offset frequencies δ_b under the application of a spin-lock pulse with the FSL of 500Hz and the TSL of 50ms. Similar to Fig. 3a, the increase of absolute offset frequency in Hz of pool B, makes it easier to recognize pool B on the Z spectrum. The MTR_{asym} curves shown in Fig. 4b illustrate that the image contrast is very small if the offset frequency of pool B is too close to the resonant frequency, while with the increasing δ_b, the maximum MTR_{asym} increases rapidly. However, when δ_b is larger than 5ppm, the maximum MTR_{asym} becomes stable, no longer increasing with δ_b (Fig. 4c). Fig. 4d shows that the location of the maximum MTR_{asym} approaches to the exact offset frequency of pool B if δ_b is sufficiently large due to the reduced direct saturation effect, indicating a better specificity.

Proton exchange rate k between pool A and B also has the effect on the Z-spectrum appearance, which is denoted in Fig. 5a. Although it may be not easy to visually recognize the apparent differences between Z-spectra at different proton exchange rates, MTR_{asym} curves for different ks shown in Fig. 5b clearly demonstrate that a more pronounced maximum MTR_{asym} could be achieved around δ_b when the FSL approximates k, similar to Fig. 1b. Note that the slight shift of the maximum MTR_{asym} may be primarily caused by the direction saturation effect since the saturation peak for pool B is so small. The MTR_{asym} at 3ppm is maximized at around 440/s (Fig. 5c), similar to the FSL of 500Hz. Meanwhile, the value of MTR_{asym} at 3ppm decreases rapidly when k is much smaller or much larger than FSL.

Figure 6 denotes the effect of a decreasing population of pool A p_a (or increasing p_b) on the overall Z-spectrum and MTR_{asym}. With the decrease of p_a, the saturation on pool B is more prominent (Fig. 6a), which overlaps with the saturation on pool A due to the relatively small δ_b of 3ppm, and broadens the peak of the overall Z-spectrum. Fig. 6b and 6c show that the maximum MTR_{asym} and the MTR_{asym} at 3ppm both increase with the larger p_b. As seen in Fig. 7c, MTR_{asym} at 3ppm is a monotonically decreasing function of p_a (note the reversed x axis).

Figure 7 denotes the effect of the population averaged T_2 on the overall Z-spectrum and MTR_{asym}. The increase of T_2 reduces the saturation rate of Z spectra (Fig. 7a), but enhances the maximum MTR_{asym} (Fig. 7b). However, the location of the maximum MTR_{asym} shifts to lower offset with the increase of T_2. As a consequence, the MTR_{asym} at 3ppm although monotonically increases with T_2, the enhancement rate is generally low (Fig. 7c).

Summary of parameter influence on Z-spectrum

The Z-spectrum of a two-pool model could be imagined as the coupling of the Z-spectra of two individual single pools through chemical exchange and spill-over effect between them (Fig. 8). The Z-spectrum of pool A reflects direct water saturation and the spectrum of the much smaller pool B is more sensitive to the chemical exchange effect. Without chemical exchange and spill-over effect, the composite two-pool Z-spectrum is exactly the sum of Z-spectrum for each single pool. In Fig. 8, Z-spectrum peak height and half width at half

maximum for two pools are defined as $h_{a,b}$ and $\Delta w_{a,b}$ respectively. The frequency difference between two peaks is defined as d. Due to chemical exchange as well as spill-over effect, d is usually smaller than $\delta_b - \delta_a$. Theoretically, h_b and Δw_b could be used to evaluate the sensitivity and specificity of chemical exchange image contrast if DS is assumed to be symmetric and its effect could be completely compensated through asymmetric analysis. For the better characterization of chemical exchange effect, a Z-spectrum with high values of h_b/h_a, $h_a/\Delta w_a$ and $h_b/\Delta w_b$ is preferable. Meanwhile, it is also preferable that $\Delta w_a + \Delta w_b << d$. The effects of each factor increase on the composite Z-spectrum appearance are summarized in Table 1 as the rule of thumb in the practical experiment settings.

Optimization of the spin-lock time and frequency for MTR_{asym} measurements

To achieve maximum MTR_{asym} and hence image contrast for chemical exchange characterization is one of the key aims for chemical exchange imaging. For CESL, adjustments of TSL, FSL and $\Delta\Omega$ could be employed for this purpose. The offset frequency of pool B usually could be determined from in vitro characterization, so is assumed to be known. For this numerical simulation, an optimal FSL was defined as the FSL that maximizes the MTR_{asym} at exactly the offset frequency of pool B (3ppm) for a specific proton exchange rate k and a fixed TSL. Optimal FSLs for proton exchange rates from 10/s to 5000/s (at a resolution of 10/s) and TSLs from 20ms to 600ms (at a resolution of 20ms) were numerically searched within the FSL range of 1Hz to 4000Hz at a search step of 1 Hz. The optimal FSLs and the corresponding maximal MTR_{asym} at 3ppm were depicted in Fig. 9 for 9.4T (a, b) and 3T (c, d), respectively. As seen in Fig. 9a and c, for both 9.4T and 3T, optimal FSL is much dependent on k when TSL is shorter than 100ms. Higher FSL is required to enhance the maximum MTR_{asym} for high proton exchange rate. In other word, FSL could be tuned to better characterize different proton exchange rates. On the other hand, when a longer TSL is applied, a lower optimal FSL is required to obtain the maximum MTR_{asym}. Meanwhile, the dependence of optimal FSL on k is also reduced. With a very long TSL like 600ms, a quite universal FSL, in particular at lower B_0 (e.g. ~130Hz at 3T), may be applied to achieve maximum MTR_{asym} for wide proton exchange rate ranges. For low to intermediate proton exchange rates, e.g. 0–500/s at 3T, the difference of the optimal FSLs is small, while this difference becomes large for high proton exchange rates. As seen in Fig. 9b and d, it is expectable that larger maximum MTR_{asym} could be achieved at 9.4T than at 3T, which may be attributed to the significantly reduced direct saturation or spill-over effect due to the increase of the absolute offset frequency of labile protons at the higher field. Overall, the greatest maximum MTR_{asym} is achieved by the optimal FSL with long TSL for low to intermediate proton exchange rates. For fast proton exchange rates, although FSL could be adjusted to enhance MTR_{asym}, the maximum MTR_{asym} values are generally quite uniform for different TSLs, and much smaller than the corresponding ones for lower proton exchange rates.

DISCUSSION

Since the Bloch-McConnell equations form the theoretical basis of chemical exchange quantification for both CEST and CESL, the theoretical derivation and simulation results shown in this study are compatible with many findings of CEST imaging in literatures.

As for the theoretical derivation, when the spin-lock pulse is applied at the offset of pool B ($\Delta\Omega = \delta_b$) for an asymmetric population two-pool system ($p_b << p_a$, $p_a \approx 1$ and $p_a p_b \approx p_b/p_a$), under the assumption of $R_2 << R_{ex}$, it is derived from Eq. [16] that:

$$M_{ss}=M_0\cdot\frac{R_1\cdot\cos\theta}{R_1\cos^2\theta+\frac{p_a p_b\delta_b{}^2 k}{\omega_1^2+k^2}\sin^2\theta}. \quad [19]$$

With the further assumption of $k<<\omega_1$ and $\omega_1<<\delta_b$ for slow exchange processes at very high field B_0, $\cos\theta\approx 1$ and $\sin\theta\approx\tan\theta=\omega_1{}^2/\delta_b{}^2$, then Eq. [19] is further simplified as:

$$\frac{M_{ss}}{M_0}\approx\frac{1}{\cos\theta+T_1\frac{p_a p_b\delta_b{}^2 k}{\omega_1^2}\tan^2\theta}\approx\frac{1}{1+T_1 p_a p_b k}\approx\frac{1}{1+T_1 k_a}=\frac{\tau_a}{\tau_a+T_1}. \quad [20]$$

Eq. [20] is exactly the Eq. [23] in the literature (Woessner *et al.*, 2005), where τ_a is the lifetime of proton in pool A, except that the average T_1 (very closed to T_{1a} due to the asymmetric population) is used in Eq. [20]. Similarly, by combining Eq. [15], it is easily derived that:

$$M=(M_0-M_{ss})\cdot e^{-R_{1\rho}\cdot TSL}+M_{ss}=M_0\left(\frac{\tau_a}{T_1+\tau_a}+\frac{T_1}{T_1+\tau_a}e^{-\frac{T_1+\tau_a}{T_1\cdot\tau_a}\cdot TSL}\right), \quad [21]$$

which is exactly the Eq. [24] for modeling of CEST in the literature (Woessner *et al.*, 2005).

Assuming no spill-over effect and $MTR(-\Delta\Omega)\approx 1$, it is also derived by substituting Eq. [21] into Eq. [18] ($\tau_a>>T_1$):

$$MTR_{asym}(\Delta\Omega)=1-\left(\frac{\tau_a}{T_1+\tau_a}+\frac{T_1}{T_1+\tau_a}e^{-\frac{T_1+\tau_a}{T_1\cdot\tau_a}\cdot TSL}\right)=\frac{T_1}{T_1+\tau_a}\left(1-e^{-\frac{T_1+\tau_a}{T_1\cdot\tau_a}\cdot TSL}\right)\approx\frac{1}{1+k_a T_1}k_a T_1\left(1-e^{-\frac{TSL}{T_1}}\right) \quad [22]$$

which is equivalent to the well-known analytical solution for CEST imaging (van Zijl and Yadav, 2011; Zhou *et al.*, 2003b; Zhou *et al.*, 2003a). The derivation of Eqs. [20–22] shows that CEST model is compatible with CESL theory, and could be considered as a simplified case of CESL model for slow exchange rate processes.

It has been also shown (Jin *et al.*, 2011) that the proposed linear plot of $M_{ss}/(M_0-M_{ss})$ versus $1/\omega_1{}^2$ (Dixon *et al.*, 2010), which could be used for concentration independent quantification of proton exchange rates in CEST, could also be derived from the asymmetric two-pool $R_{1\rho}$ model under the slow exchange assumption.

As for numerical simulation, the MTR_{asym} dependence on FSL as depicted in Fig. 1c is compatible with the theoretical analysis (Sun *et al.*, 2005) and experiment result (Sun *et al.*, 2007b) in the previous CEST studies. The MTR_{asym} dependence on TSL as depicted in Fig. 2c is also compatible with the TSL optimization analysis in the literature (Jin *et al.*, 2012). The optimal TSL occurs when $\partial MTR_{asym}/\partial TSL=0$ by using Eqs. [17–18]. For slow exchange rates and low FSL cases like those in many CEST studies, the MTR_{asym} usually monotonically increases with TSL and the optimal TSL approaches infinite. For intermediate to fast exchange rates and high FSLs, the optimal TSL becomes complicated, dependent on many factors such as T2, exchange rate and labile pool population p_b. As revealed by the two-pool $R_{1\rho}$ model, the proton exchange rate k is possible to be quantified by using the CE dependence on either FSL or TSL, consistent with the QUESP and QUEST methods proposed for CEST imaging (McMahon *et al.*, 2006). The influence of p_b on Z-spectrum is compatible with the simulation result in the literature (Zaiss *et al.*, 2012). In addition, the labile proton concentration (proportional to p_b), could also be further independently determined by using the optimal FSL (Sun, 2010).

According to the numerical simulation results in Fig. 1 to Fig. 7, it was found that the maximum MTR_{asym} does not always appear at the offset of pool B, the value and the location of the maximum MTR_{asym} could be a complicated function of many factors. MTR_{asym} at the offset of pool B encounters the similar problem. Therefore, in practice, the sensitivity and specificity of CE based image contrast, no matter by CEST or CESL, are often compromised, although could be improved by the tuning of spin-lock parameters. The interpretation of the CE based image contrast should be also very careful due to the non-monotonic nature of CE-based contrast function and the possible contrast contamination due to the spill-over effect, shifting and broadening of the Z-spectrum and the presence of multiple pools and different proton exchange rates.

B_0 and B_1 inhomogeneities could have pronounced influence on the appearance of Z-spectrum and compromise CE quantification. In particular, B_0 inhomogeneity may simulate the offset frequency of pool B, and B_1 inhomogeneity leads to the deviation of the actual FSL from the nominal FSL. Moreover, θ could be contaminated by both. Some methods have been proposed for this issue in CEST imaging (Scheidegger *et al.*, 2011; Kim *et al.*, 2009; Sun *et al.*, 2007a). For CESL, this issue could also be addressed and alleviated by the improved design of spin-lock pulses and the advanced quantification methods (Chen *et al.*, 2011; Witschey *et al.*, 2007; Charagundla *et al.*, 2003; Yuan *et al.*, 2012a).

There are some practical implications as revealed by the numerical analysis of the spin-lock pulse optimization for CESL (Fig. 9). As indicated by Fig. 9, slow, intermediate, and fast exchange may be imaged optimally with long TSL and low FSL, intermediate TSL and FSL, and short TSL and high FSL in theory, respectively, consistent with the results in a recent CESL study (Jin *et al.*, 2012). Quite similar optimal FSLs could be used to maximize the MTR_{asym} for slow to intermediate proton exchange rates (Fig. 9a, c). Meanwhile, maximum MTR_{asym} increases mainly with longer TSL in this case (Fig. 9b, d). These findings are well supported by the existing CEST studies. The strong dependence of optimal FSL on proton exchange rates (Fig. 9a, c) with short TSL is also consistent with the traditional spin-lock $T_{1\rho}$ imaging (Duvvuri *et al.*, 2001). Generally, CE image contrasts as revealed by MTR_{asym}, is much smaller for high proton exchange rates than for slow to intermediate proton exchange rates (Fig. 9b, d). Therefore, even with the optimized adjustment of FSL and TSL, it is still technically challenging to visualize the high exchange rate on image contrast by using MTR_{asym}. This challenge becomes more severe at lower B_0 field strength like 3T (Fig. 9d). By the limitation of hardware capability of a typical clinical 3T MRI scanner, a spin-lock pulse with FSL higher than 500Hz and TSL longer than 200ms may be impractical for excitation by using the body coil. Referring to the MTR_{asym} contours in Fig. 9d, an image contrast higher than 0.03 could be difficult to achieve even with the spin-lock pulse optimization, particularly for intermediate to fast CE rates (k>500/s in Fig. 9d), making the translation of CESL for clinical studies in this CE range technically challenging. Meanwhile, the strict regulation on specific absorption rate (SAR) of RF pulse has to be satisfied during patient scan for safety reason, which also imposes the difficulty of CESL for clinical studies. Numerical simulation also suggests that a large offset of pool B from water resonance and the increase of pool population ratio of labile protons by using exogenous CE agents (Zhang *et al.*, 2003; Sherry and Woods, 2008) both benefit CE contrast enhancement at clinical field strength.

The major limitation of this theoretical study is the absence of experiment for validation because there is no MRI scanner over 3T and dedicated powerful RF transmitter at our site. Therefore, theoretical derivation and numerical simulation, although compatible with previous CEST studies indirectly, should be further validated by experiments in future studies. Meanwhile, the precision of the simulation result may also be compromised by the limitation of the simplified solution for the Bloch-McCornell equations. For some particular

cases, the deviation of the simplified solution from the full Bloch numerical analysis may not be negligible. For instance, the deviation of maximum MTR_{asym} upon convergence of the two pool frequencies as shown in Fig. 4d may be carefully interpreted when the resonant frequency of pool B approaches pool A (Zaiss *et al.*, 2012). This study only discusses the effect of parameters involved in the two-pool $R_{1\rho}$ relaxation model on the Z-spectrum and MTR_{asym}. Actually, concentration of the labile proton pool (only indirectly reflected by p_b) (Zhou *et al.*, 2011), pH value (Ward and Balaban, 2000) and temperature (Zhang *et al.*, 2005) should have remarkable influence on chemical exchange and image contrast, which are not yet discussed in this study. In practice, cross-relaxation (Davis and Bax, 1985), represented by nuclear Overhauser enhancement (NOE) effect (Ling *et al.*, 2008) may also contaminate Z-spectrum and compromise MTR_{asym} analysis. It is also not involved in the $R_{1\rho}$ model used in this study and has to be investigated in future experimental studies. The results in this study are only valid for a two-pool model. The extension to multi-pool model should be further developed in the future.

In summary, CESL, an alternative to CEST, should be promising as a powerful chemical exchange imaging tool. In this study, Z-spectrum and asymmetric MTR obtained by CESL are theoretically analyzed and numerically simulated using a general two-pool $R_{1\rho}$ relaxation model outside of fast-exchange limit. The influence of spin-lock parameters, B_0 field strength and physiological properties on CESL Z-spectrum and MTR_{asym} are quantitatively revealed. Theoretical analysis shows that the classical analytical CEST model could also be derived from the $R_{1\rho}$ relaxation model for CESL. Numerical simulation results in this study are compatible with and well supported by the existing chemical exchange imaging studies. Further experimental validations of CESL should be performed in future studies.

Acknowledgments

This work is supported by Hong Kong RGC grants CUHK475911, CUHK418811 and SEG_CUHK02 and a US National Institutes of Health grant R01EB009731.

REFERENCES

Borthakur A, Sochor M, Davatzikos C, Trojanowski JQ, Clark CM. T1rho MRI of Alzheimer's disease. Neuroimage. 2008; 41:1199–1205. [PubMed: 18479942]

Cai K, Haris M, Singh A, Kogan F, Greenberg JH, Hariharan H, Detre JA, Reddy R. Magnetic resonance imaging of glutamate. Nat Med. 2012; 18:302–306. [PubMed: 22270722]

Charagundla SR, Borthakur A, Leigh JS, Reddy R. Artifacts in T(1rho)-weighted imaging: correction with a self-compensating spin-locking pulse. J Magn Reson. 2003; 162:113–121. [PubMed: 12762988]

Chen W, Takahashi A, Han E. Quantitative T(1)(rho) imaging using phase cycling for B(0) and B(1) field inhomogeneity compensation. Magn Reson Imaging. 2011; 29:608–619. [PubMed: 21524869]

Davis DG, Bax A. Separation of Chemical-Exchange and Cross-Relaxation Effects in Two-Dimensional Nmr-Spectroscopy. Journal of Magnetic Resonance. 1985; 64:533–535.

Desvaux H, Berthault P. Study of dynamic processes in liquids using off-resonance rf irradiation. Prog Nucl Mag Res Sp. 1999; 35:295–340.

Dixon WT, Ren J, Lubag AJ, Ratnakar J, Vinogradov E, Hancu I, Lenkinski RE, Sherry AD. A concentration-independent method to measure exchange rates in PARACEST agents. Magn Reson Med. 2010; 63:625–632. [PubMed: 20187174]

Duvvuri U, Goldberg AD, Kranz JK, Hoang L, Reddy R, Wehrli FW, Wand AJ, Englander SW, Leigh JS. Water magnetic relaxation dispersion in biological systems: the contribution of proton exchange and implications for the noninvasive detection of cartilage degradation. Proc Natl Acad Sci U S A. 2001; 98:12479–12484. [PubMed: 11606754]

Jin T, Autio J, Obata T, Kim SG. Spin-locking versus chemical exchange saturation transfer MRI for investigating chemical exchange process between water and labile metabolite protons. Magn Reson Med. 2011; 65:1448–1460. [PubMed: 21500270]

Jin T, Wang P, Zong X, Kim SG. Magnetic resonance imaging of the Amine-Proton EXchange (APEX) dependent contrast. Neuroimage. 2012; 59:1218–1227. [PubMed: 21871570]

Johannessen W, Auerbach JD, Wheaton AJ, Kurji A, Borthakur A, Reddy R, Elliott DM. Assessment of human disc degeneration and proteoglycan content using T1rho-weighted magnetic resonance imaging. Spine (Phila Pa 1976). 2006; 31:1253–1257. [PubMed: 16688040]

Kim M, Gillen J, Landman BA, Zhou J, van Zijl PC. Water saturation shift referencing (WASSR) for chemical exchange saturation transfer (CEST) experiments. Magn Reson Med. 2009; 61:1441–1450. [PubMed: 19358232]

Kogan F, Singh A, Cai K, Haris M, Hariharan H, Reddy R. Investigation of chemical exchange at intermediate exchange rates using a combination of chemical exchange saturation transfer (CEST) and spin-locking methods (CESTrho). Magn Reson Med. 2012; 68:107–119. [PubMed: 22009759]

Li X, Han ET, Busse RF, Majumdar S. In vivo T(1rho) mapping in cartilage using 3D magnetization-prepared angle-modulated partitioned k-space spoiled gradient echo snapshots (3D MAPSS). Magn Reson Med. 2008; 59:298–307. [PubMed: 18228578]

Ling W, Regatte RR, Navon G, Jerschow A. Assessment of glycosaminoglycan concentration in vivo by chemical exchange-dependent saturation transfer (gagCEST). Proc Natl Acad Sci U S A. 2008; 105:2266–2270. [PubMed: 18268341]

McMahon MT, Gilad AA, Zhou J, Sun PZ, Bulte JW, van Zijl PC. Quantifying exchange rates in chemical exchange saturation transfer agents using the saturation time and saturation power dependencies of the magnetization transfer effect on the magnetic resonance imaging signal (QUEST and QUESP): Ph calibration for poly-L-lysine and a starburst dendrimer. Magn Reson Med. 2006; 55:836–847. [PubMed: 16506187]

Scheidegger R, Vinogradov E, Alsop DC. Amide proton transfer imaging with improved robustness to magnetic field inhomogeneity and magnetization transfer asymmetry using saturation with frequency alternating RF irradiation. Magn Reson Med. 2011; 66:1275–1285. [PubMed: 21608029]

Sherry AD, Woods M. Chemical exchange saturation transfer contrast agents for magnetic resonance imaging. Annual Review of Biomedical Engineering. 2008; 10:391–411.

Stanisz GJ, Odrobina EE, Pun J, Escaravage M, Graham SJ, Bronskill MJ, Henkelman RM. T1, T2 relaxation and magnetization transfer in tissue at 3T. Magn Reson Med. 2005; 54:507–512. [PubMed: 16086319]

Sun PZ. Simultaneous determination of labile proton concentration and exchange rate utilizing optimal RF power: Radio frequency power (RFP) dependence of chemical exchange saturation transfer (CEST). MRI J Magn Reson. 2010; 202:155–161.

Sun PZ, Farrar CT, Sorensen AG. Correction for artifacts induced by B(0) and B(1) field inhomogeneities in pH-sensitive chemical exchange saturation transfer (CEST) imaging. Magn Reson Med. 2007a; 58:1207–1215. [PubMed: 17969015]

Sun PZ, van Zijl PC, Zhou J. Optimization of the irradiation power in chemical exchange dependent saturation transfer experiments. J Magn Reson. 2005; 175:193–200. [PubMed: 15893487]

Sun PZ, Zhou J, Huang J, van Zijl P. Simplified quantitative description of amide proton transfer (APT) imaging during acute ischemia. Magn Reson Med. 2007b; 57:405–410. [PubMed: 17260362]

Trott O, Palmer AG 3rd. R1rho relaxation outside of the fast-exchange limit. J Magn Reson. 2002; 154:157–160. [PubMed: 11820837]

van Zijl PC, Yadav NN. Chemical exchange saturation transfer (CEST): what is in a name and what isn't? Magn Reson Med. 2011; 65:927–948. [PubMed: 21337419]

Wang YX, Yuan J, Chu ES, Go MY, Huang H, Ahuja AT, Sung JJ, Yu J. T1rho MR Imaging Is Sensitive to Evaluate Liver Fibrosis: An Experimental Study in a Rat Biliary Duct Ligation Model. Radiology. 2011; 259:712–719. [PubMed: 21436087]

Ward KM, Aletras AH, Balaban RS. A new class of contrast agents for MRI based on proton chemical exchange dependent saturation transfer (CEST). J Magn Reson. 2000; 143:79–87. [PubMed: 10698648]

Ward KM, Balaban RS. Determination of pH using water protons and chemical exchange dependent saturation transfer (CEST). Magn Reson Med. 2000; 44:799–802. [PubMed: 11064415]

Witschey WR 2nd, Borthakur A, Elliott MA, Mellon E, Niyogi S, Wallman DJ, Wang C, Reddy R. Artifacts in T1 rho-weighted imaging: compensation for B(1) and B(0) field imperfections. J Magn Reson. 2007; 186:75–85. [PubMed: 17291799]

Woessner DE, Zhang S, Merritt ME, Sherry AD. Numerical solution of the Bloch equations provides insights into the optimum design of PARACEST agents for MRI. Magn Reson Med. 2005; 53:790–799. [PubMed: 15799055]

Yuan J, Li Y, Zhao F, Chan Q, Ahuja AT, Wang YX. Quantification of T1rho relaxation by using rotary echo spin-lock pulses in the presence of B0 inhomogeneity. Phys Med Biol. 2012a; 57:5003–5016. [PubMed: 22805278]

Yuan J, Zhao F, Griffith JF, Chan Q, Wang YX. Optimized efficient liver T1rho mapping using limited spin lock times. Phys Med Biol. 2012b; 57:1631–1640. [PubMed: 22398137]

Zaiss M, Bachert P. Equivalence of spin-lock and magnetization transfer NMR experiments. 2012 http://arxiv.org/abs/1203.2067.

Zaiss M, Schnurr M, Bachert P. Analytical solution for the depolarization of hyperpolarized nuclei by chemical exchange saturation transfer between free and encapsulated xenon (HyperCEST). Journal of Chemical Physics. 2012; 136

Zhang S, Malloy CR, Sherry AD. MRI thermometry based on PARACEST agents. J Am Chem Soc. 2005; 127:17572–17573. [PubMed: 16351064]

Zhang S, Merritt M, Woessner DE, Lenkinski RE, Sherry AD. PARACEST agents: modulating MRI contrast via water proton exchange. Acc Chem Res. 2003; 36:783–790. [PubMed: 14567712]

Zhou J, Lal B, Wilson DA, Laterra J, van Zijl PC. Amide proton transfer (APT) contrast for imaging of brain tumors. Magn Reson Med. 2003a; 50:1120–1126. [PubMed: 14648559]

Zhou J, Tryggestad E, Wen Z, Lal B, Zhou T, Grossman R, Wang S, Yan K, Fu DX, Ford E, Tyler B, Blakeley J, Laterra J, van Zijl PC. Differentiation between glioma and radiation necrosis using molecular magnetic resonance imaging of endogenous proteins and peptides. Nat Med. 2011; 17:130–134. [PubMed: 21170048]

Zhou J, Wilson DA, Sun PZ, Klaus JA, Van Zijl PC. Quantitative description of proton exchange processes between water and endogenous and exogenous agents for WEX, CEST, and APT experiments. Magn Reson Med. 2004; 51:945–952. [PubMed: 15122676]

Zhou JY, Payen JF, Wilson DA, Traystman RJ, van Zijl PCM. Using the amide proton signals of intracellular proteins and peptides to detect pH effects in MRI. Nature Medicine. 2003b; 9:1085–1090.

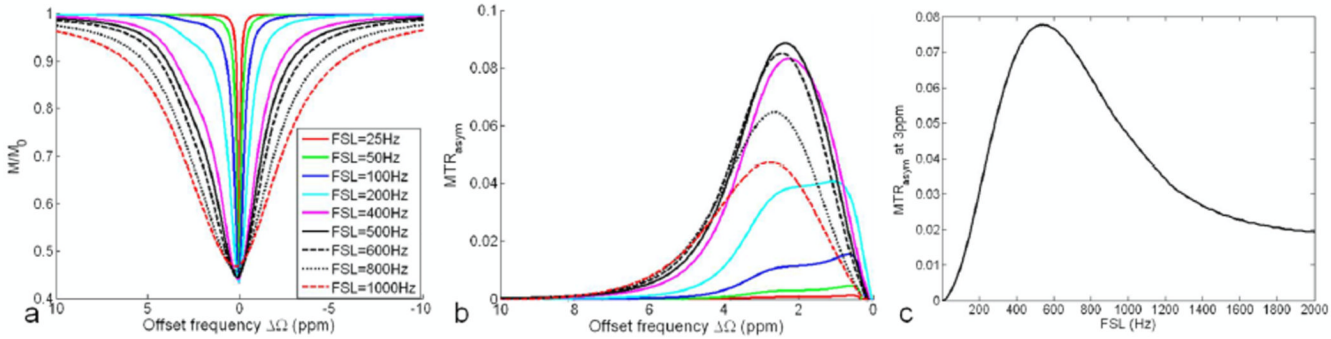

Fig. 1.

Simulated Z-spectrum (a) and MTR_{asym} (b) for a two-pool system (p_a=0.99, p_b=0.01, δ_b=3ppm) under the application of spin-lock pulses with different FSLs but a fixed TSL of 50ms at 9.4T. The variation of MTR_{asym} at the 3ppm offset of pool B versus FSL is illustrated in (c).

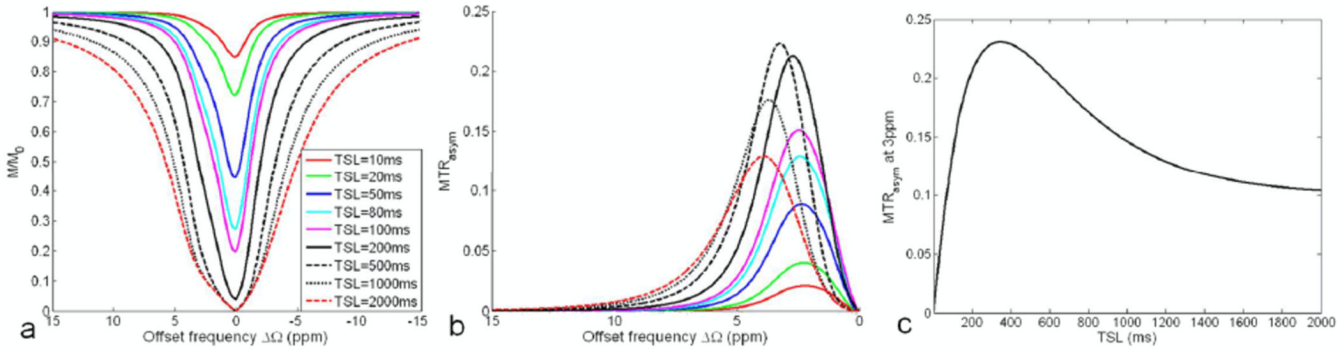

Fig. 2.

Simulated Z-spectrum (a) and MTR_{asym} (b) for a two-pool system (p_a=0.99, p_b=0.01, δ_b=3ppm) under the application of spin-lock pulses with different TSLs but a fixed FSL of 500Hz at 9.4T. The variation of MTR_{asym} at the 3ppm offset of pool B versus TSL is illustrated in (c).

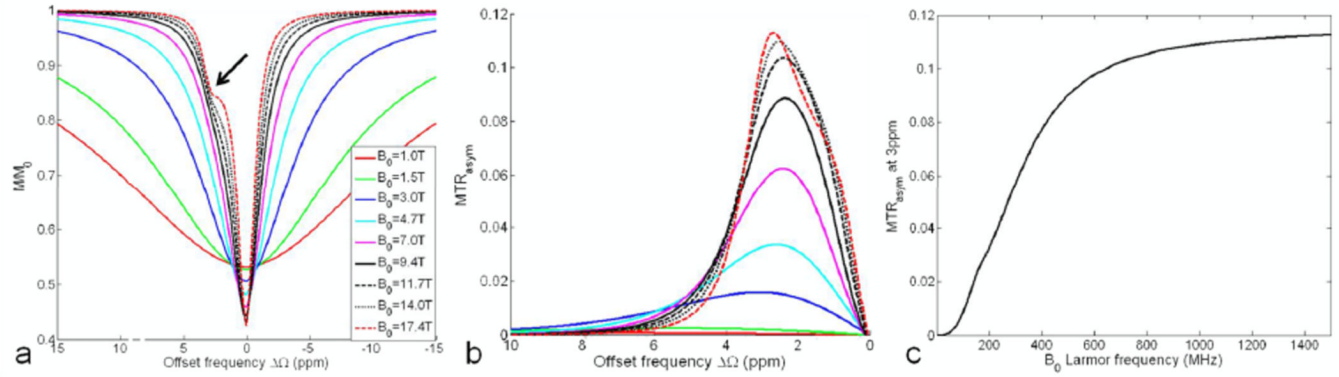

Fig. 3.

Simulated Z-spectrum (a) and MTR_{asym} (b) for a two-pool system (p_a=0.99, p_b=0.01, δ_b=3ppm) under the application of a spin-lock pulse (FSL=500Hz, TSL=50ms) at different B_0. (c) MTR_{asym} at the 3ppm offset of pool B versus TSL is always increasing with B_0.

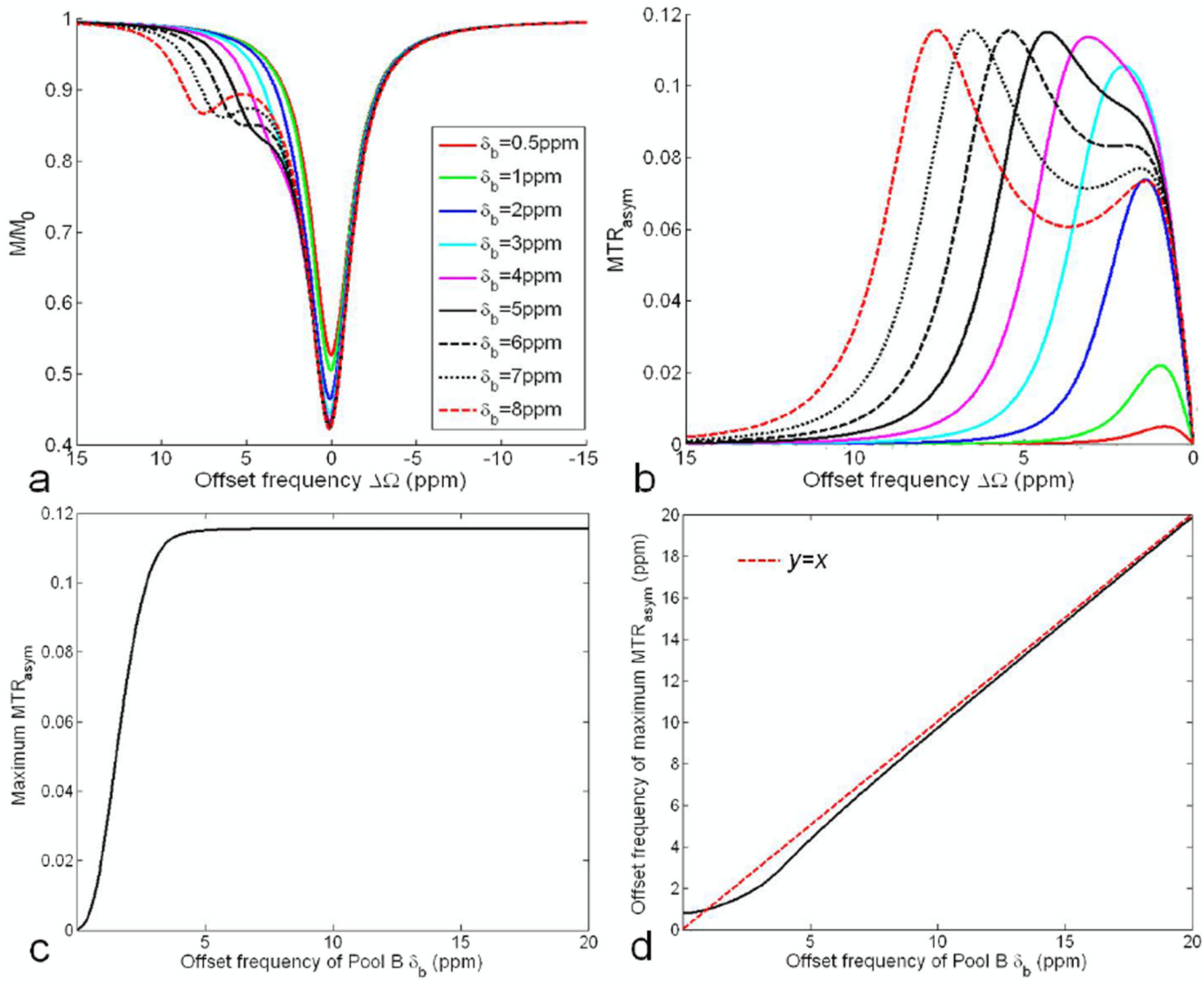

Fig. 4.

Simulated Z-spectrum (a) and MTR_{asym} (b) for a two-pool system (p_a=0.99, p_b=0.01) under the application of a spin-lock pulse (FSL=500Hz, TSL=50ms) at 9.4T when pool B resonates at different offset frequencies δ_b. (c) Variation of maximum MTR_{asym} versus δ_b. (d) The location of maximum MTR_{asym} approaches the exact offset frequency of pool B with increasing δ_b.

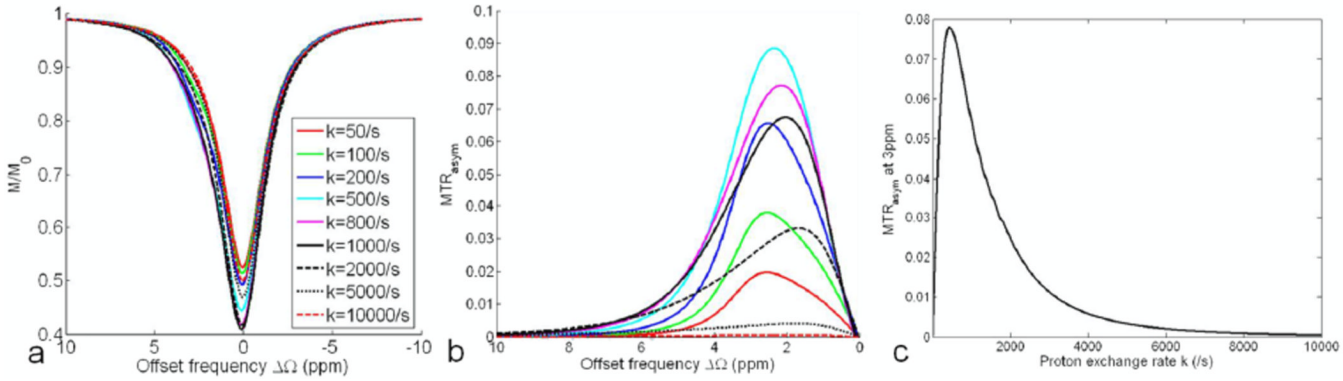

Fig. 5.

Simulated Z-spectrum (a) and MTR_{asym} (b) for a two-pool system (p_a=0.99, p_b=0.01, δ_b=3ppm) under the application of a spin-lock pulse (FSL=500Hz, TSL=50ms) at 9.4T for different proton exchange rates *k*. (c) MTR_{asym} at 3ppm versus k first increases and then decreases with *k*.

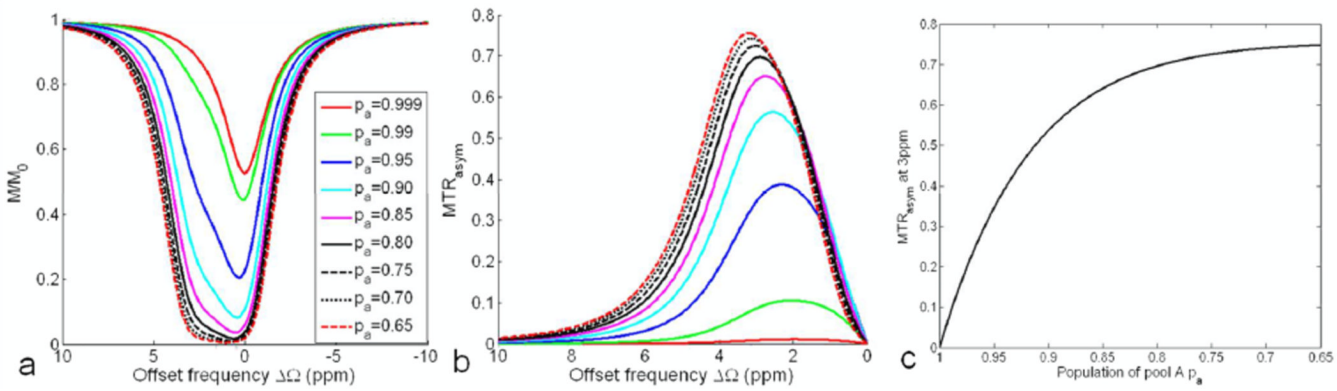

Fig. 6.

Simulated Z-spectrum (a) and MTR_{asym} (b) for a two-pool system (δ_b=3ppm) under the applications of a spin-lock pulse (FSL=500Hz, TSL=50ms) at 9.4T. (c) MTR_{asym} at 3ppm decreases monotonically with p_a (note the reversed x axis).

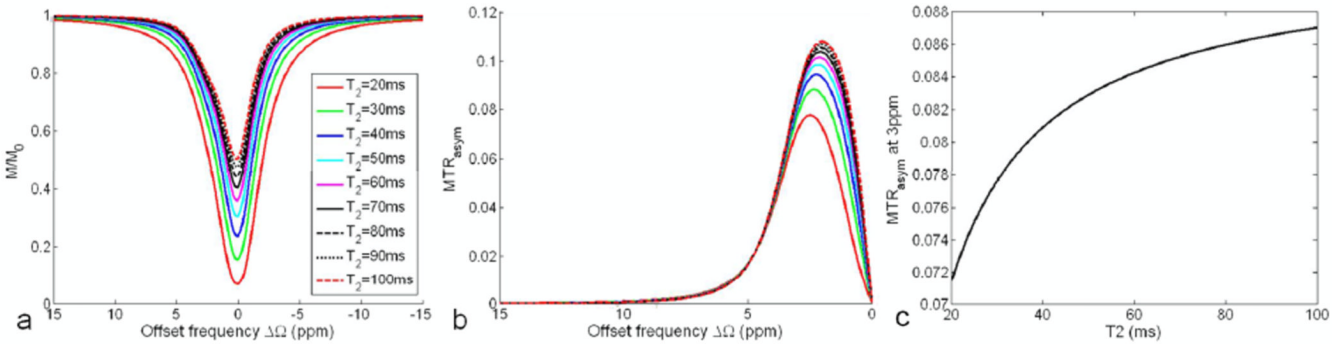

Fig. 7.

Simulated Z-spectrum (a) and MTR_{asym} (b) for a two-pool system (p_a=0.99, p_b=0.01, δ_b=3ppm) with different population-averaged T_2 values under the application of a spin-lock pulse (FSL=500Hz, TSL=50ms) at 9.4T. (c) MTR_{asym} at 3ppm increases monotonically with the population averaged T_2.

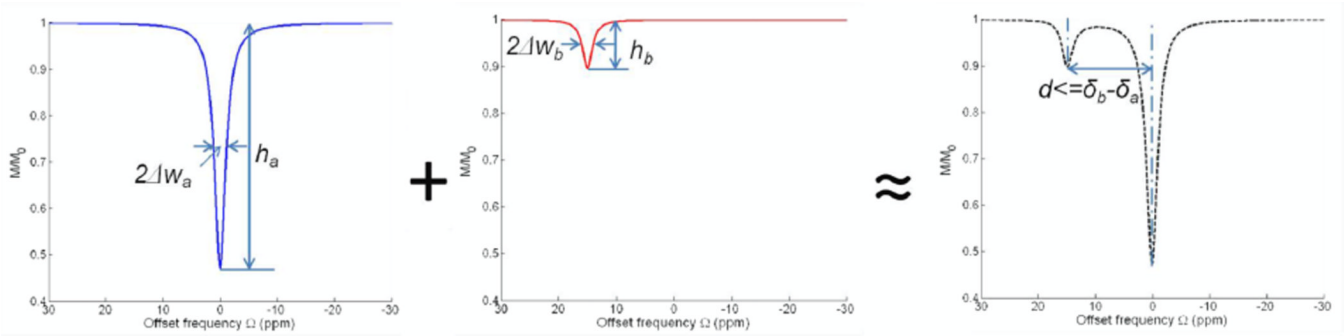

Fig. 8.

The overall Z-spectrum can be considered as the composition and coupling of two individual Z-spectra of pool A and B under the chemical exchange and spill-over effect. An ideal Z-spectrum for better characterization of chemical exchange should have high values of h_b/h_a, $h_a/\Delta w_a$ and $h_b/\Delta w_b$. $\Delta w_a+\Delta w_b$ is preferable to be much smaller than the saturation peak difference d as well.

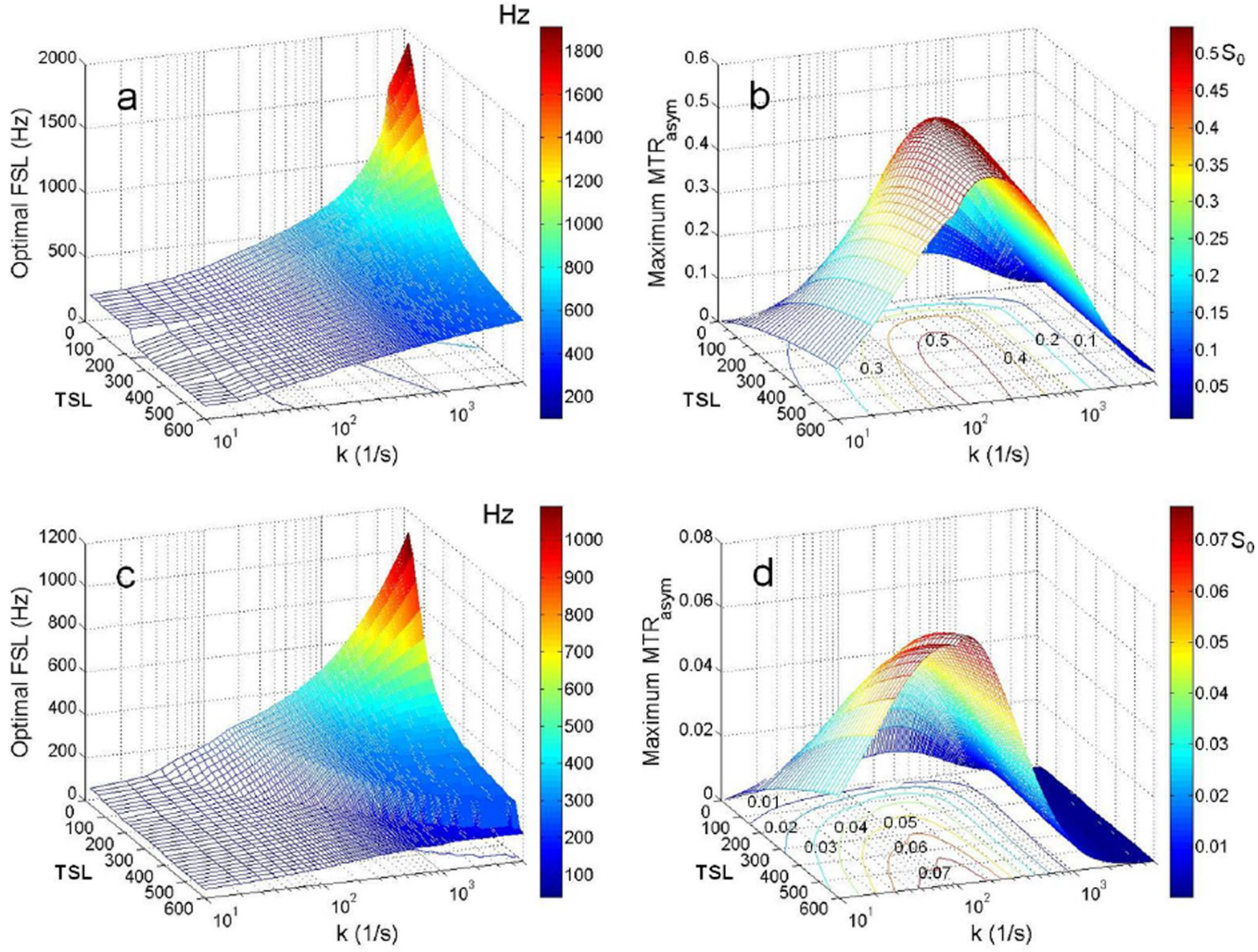

Fig. 9.

The optimal FSL and the corresponding maximal MTR_{asym} at 3ppm achieved for different proton exchange rates k and different TSLs at 9.4T and 3T. (a) Optimal FSL at 9.4T; (b) maximal MTR_{asym} achieved by the optimal FSL at 9.4T; (c) optimal FSL at 3T; (b) maximal MTR_{asym} achieved by the optimal FSL at 3T. The contours plotted in the transverse plane in (b) and (d) are labeled with the level of the maximal $MTR_{asym.}$ The area inside a contour has the maximal MTR_{asym} values higher than the corresponding level.

Table. 1

The summary of the effect of each increasing factor on the composite Z-spectrum.

	h_a	Δw_a	$h_a/\Delta w_a$	h_b	Δw_b	$h_b/\Delta w_b$	h_b/h_a	d(ppm)
FSL	↑→	↑	↓	↑	↑	↑↓	↑	→↓
TSL	↑→	↑	→↓	↑→	↑	→↓	→↑	→
B_0	→	↓	↑	→	↓	↑	→	↑→
δ_b	→	→	→	→	→	→	→	↑
k	↑↓	↑↓	→	↑↓	↑	↑↓	↑↓	→
p_b	↑	↑	→	↑	↑	↑→	↑	→
T_2	↓	↓	→	→	→	→	↑	→

↑, ↓, and → indicate increase, decrease and no or very small change, respectively. ↑↓ indicate increase first and then decrease, and so on. Note that this table only provides the rough guideline and is applicable for the situations when two pool peaks are recognizable on the composite Z-spectrum.